ADVANCED MATERIALS
www.advmat.de

Stable and High-Power Calcium-Ion Batteries Enabled by Calcium Intercalation into Graphite

*Jooha Park, Zheng-Long Xu, Gabin Yoon, Sung Kwan Park, Jian Wang, Hyejeong Hyun, Hyeokjun Park, Jongwoo Lim, Yoon-Joo Ko, Young Soo Yun, and Kisuk Kang**

Calcium-ion batteries (CIBs) are considered to be promising next-generation energy storage systems because of the natural abundance of calcium and the multivalent calcium ions with low redox potential close to that of lithium. However, the practical realization of high-energy and high-power CIBs is elusive owing to the lack of suitable electrodes and the sluggish diffusion of calcium ions in most intercalation hosts. Herein, it is demonstrated that calcium-ion intercalation can be remarkably fast and reversible in natural graphite, constituting the first step toward the realization of high-power calcium electrodes. It is shown that a graphite electrode exhibits an exceptionally high rate capability up to 2 A g^{-1}, delivering ≈75% of the specific capacity at 50 mA g^{-1} with full calcium intercalation in graphite corresponding to ≈97 mAh g^{-1}. Moreover, the capacity stably maintains over 200 cycles without notable cycle degradation. It is found that the calcium ions are intercalated into graphite galleries with a staging process. The intercalation mechanisms of the "calciated" graphite are elucidated using a suite of techniques including synchrotron in situ X-ray diffraction, nuclear magnetic resonance, and first-principles calculations. The versatile intercalation chemistry of graphite observed here is expected to spur the development of high-power CIBs.

Recently, exhaustive efforts have been devoted to exploring new energy storage systems with higher energy density, longer life, and lower cost than that offered by current lithium-ion batteries to cope with the growing demand for electric vehicles and the storage of electricity from renewable energy sources.[1] Multivalent ion batteries are considered promising alternatives owing to the doubled or tripled electron exchange per charge carrier, potentially leading to both higher energy density and power density.[2–8] Specifically, Mg^{2+},[2,3,9] Al,[3+][4] and Ca^{2+}[6–8] have attracted intensive interest in the research community because of their natural abundance, lightweight, and stable multivalent states. Moreover, an electrochemical system employing calcium is capable of offering the highest voltage among these systems with a reduction potential (−2.9 V vs standard hydrogen electrode, SHE) that is lower than that of magnesium (−2.4 V vs SHE) and aluminum (−1.7 V vs SHE), and comparable to that of lithium (−3.0 V vs SHE), implying the potential promise of calcium-ion batteries (CIBs).[3,6–8] Nevertheless, progress in the development of CIBs has thus far been stalled by several fundamental challenges. i) The use of Ca metal as an anode is not trivial owing to the ion-blocking solid electrolyte interphase (SEI) formed at the surface of Ca metal in conventional electrolytes.[6–8,10] ii) In addition, the diffusion kinetics of divalent calcium ions within intercalation hosts is unacceptably sluggish arising from the strong electrostatic interaction between Ca^{2+} and the host structure, thereby leading to poor rate performance of CIBs.[11,12] iii) Finally, the multivalent calcium ions generally form a strong solvation

J. Park, Dr. Z.-L. Xu, Dr. G. Yoon, S. K. Park, Dr. H. Park, Prof. K. Kang
Department of Materials Science and Engineering
Research Institute of Advanced Materials (RIAM)
Seoul National University
1 Gwanak-ro Gwanak-gu, Seoul 151–742, Republic of Korea
E-mail: matlgen1@snu.ac.kr

Dr. J. Wang, H. Hyun, Prof. J. Lim
Department of Chemistry
Seoul National University
1 Gwanak-ro Gwanak-gu, Seoul 151–742, Republic of Korea

Dr. Y.-J. Ko
Lab of Nuclear Magnetic Resonance
National Center for Inter-University Research Facilities
Seoul National University
Seoul 08826, Republic of Korea

The ORCID identification number(s) for the author(s) of this article can be found under https://doi.org/10.1002/adma.201904411.

Prof. Y. S. Yun
KU-KIST Graduate School of Converging Science and Technology
Korea University
Seoul 02841, Republic of Korea

Prof. K. Kang
Institute of Engineering Research
College of Engineering
Seoul National University
1 Gwanak-ro Gwanak-gu, Seoul 151–742, Republic of Korea

Prof. K. Kang
Center for Nanoparticle Research
Institute of Basic Science
Seoul National University
1 Gwanak-ro Gwanak-gu, Seoul 151–742, Republic of Korea

DOI: 10.1002/adma.201904411

structure with solvent molecules in the electrolyte; thus, high energy is required to break the solvation, resulting in slow charge-transfer kinetics during intercalation.[6,11] In this respect, the discovery of a calcium host material or strategy that can mitigate these issues has long been awaited.

Graphite is one of the most well-known anode materials for lithium-ion batteries because of the capability of reversible lithium intercalation.[13] The reversible and fast intercalation of lithium in graphite at a low potential along with its low cost has made graphite the most commercially successful material for lithium-battery chemistry. Early studies demonstrated that graphite could also accommodate a wide range of other guest species, including multivalent ions such as magnesium, calcium, barium, and aluminum, forming graphite intercalation compounds (GICs) under certain conditions.[14] In addition, large anions, such as PF_6^-, $CF_3SO_3^-$, and $AlCl_4^-$, have also been reversibly (de)intercalated in graphite galleries, constructing high-voltage and high-energy dual ion batteries.[15] Emery et al. showed that a Ca-based GIC with the stoichiometry of CaC_6 could be chemically synthesized using highly oriented pyrolytic graphite and molten Li–Ca alloy at 350 °C.[16] More recently, Xu and Lerner reported that ternary GICs composed of alkaline-earth metals and organic molecules can be synthesized at milder temperatures of 25–100 °C.[17] Although these studies suggest that graphite may allow calcium intercalation at relatively high temperature, the formation of Ca-based GICs under ambient conditions has not yet been proven. Moreover, it remains to be observed whether reversible de/intercalation of calcium ions in a graphite host is possible, which would serve as a basis for the electrochemical calcium storage in the graphite. Considering the wide applicability with low cost and proven success of graphite electrodes in lithium-ion batteries, the application of graphite as a reversible calcium-ion host would be an important milestone toward the realization of room-temperature CIBs.

Herein, we demonstrate that reversible calcium intercalation into graphite is feasible in a room-temperature electrochemical system when an appropriate electrolyte is selected and the solvation of calcium ions is strengthened. An elaborate search of various combinations of calcium salts and solvating agents is conducted, and a dimethylacetamide (DMAc)-based electrolyte is shown to enable the intercalation of calcium ions into graphite by forming a $[Ca\text{-}(DMAc)_4]C_{50}$ ternary GIC. Moreover, we reveal that the intercalation of calcium into the graphite electrode is remarkably reversible and kinetically fast, which enables the electrochemical cycling of the graphite electrode over 200 cycles with negligible capacity fading as well as a high rate capability sustained up to 2 A g^{-1}. The detailed intercalation processes and structures of the calciated graphite are elucidated by synchrotron in situ X-ray diffraction (XRD), ex situ Raman spectroscopy, Fourier-transform infrared (FTIR) spectroscopy, and ^{13}C nuclear magnetic resonance (NMR) spectroscopy characterization along with density functional theory (DFT) calculations.

Figure 1a presents a schematic illustration of the electrochemical cell with natural graphite as the working electrode, a Ca metal counter electrode, and a 0.5 M $Ca(BH_4)_2$ DMAc electrolyte. We first performed galvanostatic discharging/charging of the cell at 50 mA g^{-1} between 0.2 and 1.5 V versus Ca^{2+}/Ca. The graphite electrode exhibited an initial discharge capacity of

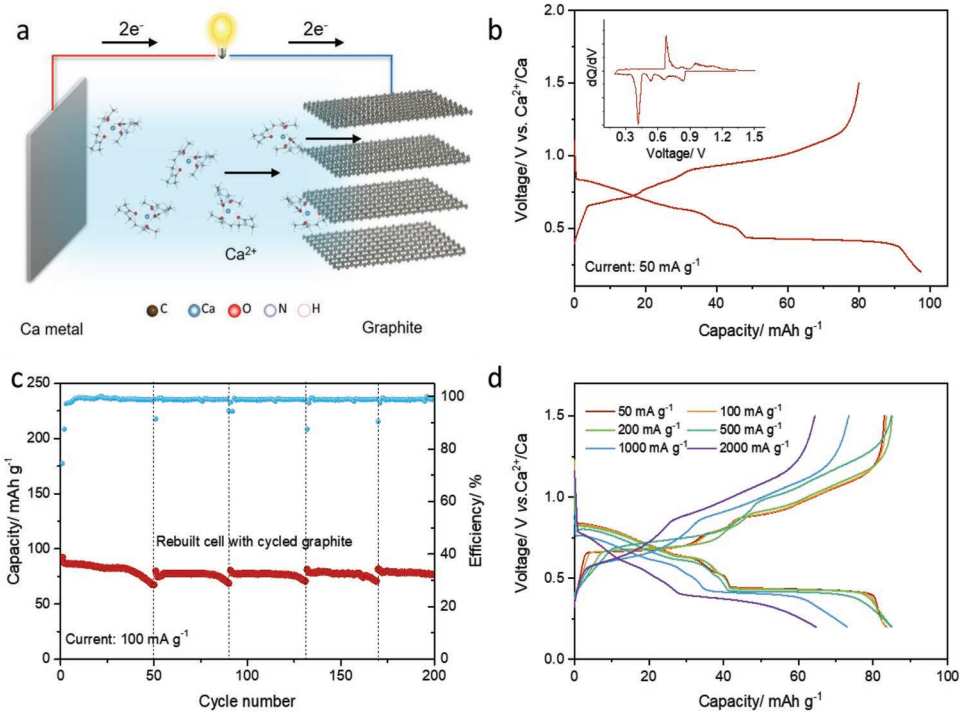

Figure 1. Electrochemical performance of graphite anode in Ca-ion battery. a) Schematic of Ca-ion intercalation in graphite during discharging. b) Initial discharge/charge voltage profile of graphite anode at 50 mA g^{-1} between 0.2 and 1.5 V, inset image showing the corresponding dQ/dV curve. c) Cyclic capacities and Coulombic efficiencies at 100 mA g^{-1}, note that after 50 cycles, the cells with cycled graphite electrode were rebuilt with fresh electrolyte and Ca metal every 40 cycles. d) Rate capacities from 50 to 2000 mA g^{-1}.

97 mAh g^{-1} and a Coulombic efficiency of 83.5% (Figure 1b). A few plateaus are apparent in the discharge/charge profile, implying a series of two-phase reactions involving stable intermediate phases during the electrochemical reaction.[18] Notably, several cathodic and anodic peaks are evident and reversibly displayed in the dQ/dV curve (inset Figure 1b), further suggesting multiple phase reactions, to be discussed later. It is worth noting that the feasibility of calcium intercalation into a graphite electrode strongly depends on the nature of the solvent. Negligible capacities were obtained when we tested acetonitrile (ACN), diethylene glycol dimethyl ether (DEGDME), tetrahydrofuran (THF), and ethylene carbonate/dimethyl carbonate (EC/DMC) solvents containing 0.5 M $Ca(BH_4)_2$ salt as electrolytes (Figure S1, Supporting Information). Raman spectra show that DMAc possesses the strongest solvation with $Ca(BH_4)_2$ among these solvents (Figure S2, Supporting Information), which would favor the intercalation of Ca ion with DMAc molecules, to be discussed later.

Figure 1c,d and Figure S3 (Supporting Information) show the cyclic stability and rate capabilities of graphite electrodes in a calcium electrochemical cell. At a current density of 100 mA g^{-1}, a discharge capacity of ≈87 mAh g^{-1} remained stable with Coulombic efficiencies of 99.5% after a few cycles. Up to 95% of the initial capacity was retained after 40 cycles, indicating the high reversibility of the electrochemical reaction; however, discernible capacity degradation was observed from 40 to 50 cycles (Figure 1c). We suspected that the capacity fade after 40 cycles may have primarily originated from the degradation of the Ca metal counter electrode rather than being due to instability of the graphite electrode itself. Indeed, postmortem analysis of the cycled cells revealed that Ca metal was severely etched and covered with C- and O-rich passivation layers (Figure S5, Supporting Information), whereas the graphite electrode remained almost intact (Figure S4, Supporting Information). This finding is consistent with the conclusion of previous reports that the passivation layer on Ca metal gradually inhibits calcium-ion transport, causing the failure of reversible Ca stripping and plating reactions.[6,8] To verify whether the unstable Ca metal induced the cyclic instability of the cells, we reassembled the cycled graphite with a fresh Ca metal electrode. Interestingly, the original capacity could be recovered for another 40 cycles with high capacity retention in the rebuilt cell. Thus, the cycle life could be extended to more than 200 cycles (Figure 1c), indicating the impressive reversibility of the graphite electrode in the calcium electrochemical cell. XRD patterns of 250 times cycled graphite electrodes present slightly broadended (002) peak (Figure S6, Supporting Information), which may also induce capacity fade for long-term cycles. Additionally, the rate capability of the graphite electrode was investigated by probing the charging/discharging responses at different current densities, as shown in Figure 1d. Unexpectedly, even upon increasing the current density by 40-folds from 50 to 2000 mA g^{-1}, as much as 75% of the specific capacity could be retained with only a small reduction of the capacity from 89 to 67 mAh g^{-1}. It is noteworthy that the rate capability demonstrated here far outperforms that of a recently reported hybrid dual-ion cell based on a Ca_7Sn_6 electrode, which delivered a capacity of 40 mAh g^{-1} at a current density of 400 mA g^{-1}.[7] More detailed analyses of the kinetic properties of the graphite electrode are presented in Figure S7 (Supporting Information). Furthermore, X-ray photoelectron spectroscopy (XPS) spectra (Figure S8, Supporting Information) and high-resolution transmission electron microscopy (HR-TEM) images (Figure S9, Supporting Information) of cycled electrode clarified no presence of SEI layers, which may contribute to fast reaction kinetics by reducing charge transfer resistance during de/intercalation reaction.[19]

To determine the electrochemical activity of graphite in a room-temperature calcium cell, the structural evolution of the graphite electrode was probed by synchrotron in situ XRD using an in-house-designed pouch-type cell. XRD patterns were periodically collected approximately every 5 min simultaneously with galvanostatic cycling at 25 mA g^{-1}.[20] The full diffractograms are provided in Figure S10 (Supporting Information) along with the cell configuration for the XRD study. **Figure 2** presents an augmented view of the evolution of the XRD peaks of graphite over the electrochemical cycle, revealing that the discharge/charge was accompanied by highly reversible structural transformation of graphite, a testament to the calciation of the graphite electrode and its excellent reversibility (additional Raman experimental evidence of the reversible structural change is provided in Figure S11 in the Supporting Information). A more detailed examination of the evolution of the XRD patterns in Figure 2 reveals that the typical staging behavior of a layered intercalation host occurs during electrochemical calcium insertion and extraction. During the early stage of discharging, the (002) main peak at 26.5° corresponding to the pristine graphite split into two new peaks, one at a larger angle and the other at a smaller angle, which continued to shift to larger or lower angles until they remain constant at 25.1° and 29.7°, respectively, forming a stage n GIC. Between 0.54 and 0.41 V of calciation, a biphasic reaction began to occur, leading to the formation of another phase of a stage o GIC with two peaks at 19.7° and 24.8° at the expense of the stage n GIC. After the completion of the biphasic reaction into the stage o GIC, a stage p GIC with two peaks at 18.3° and 24.4° appeared. In the subsequent final intercalation reactions, only a stage p GIC was observed with no significant change in the XRD pattern. The relations among the n, o, and p stages will be discussed later. Upon charging the cell, reverse reactions clearly occurred, leading to the gradual disappearance of the stage p GIC and re-formation of the stage o and n GICs. When fully charged at 1.5 V, the main (002) peak for pristine graphite was recovered, signifying the reversibility of the calciation/decalciation reactions. Noteworthy is that the weak intensity of pristine graphite peak (002) is attributable to the thin electrode and the in-house-designed pouch cell configuration.

The Miller indices (l) for the XRD peaks were determined by applying Bragg's law using the following equations[18]

$$d_{00l} = \frac{I_c}{l}; d_{00l+1} = \frac{I_c}{l+1} \tag{1}$$

$$d_{00l} \sin\theta_{00l} = d_{00l+1} \sin\theta_{00l+1} \tag{2}$$

$$l = \frac{1}{\left(\frac{\sin\theta_{00l+1}}{\sin\theta_{00l}} - 1\right)} \tag{3}$$

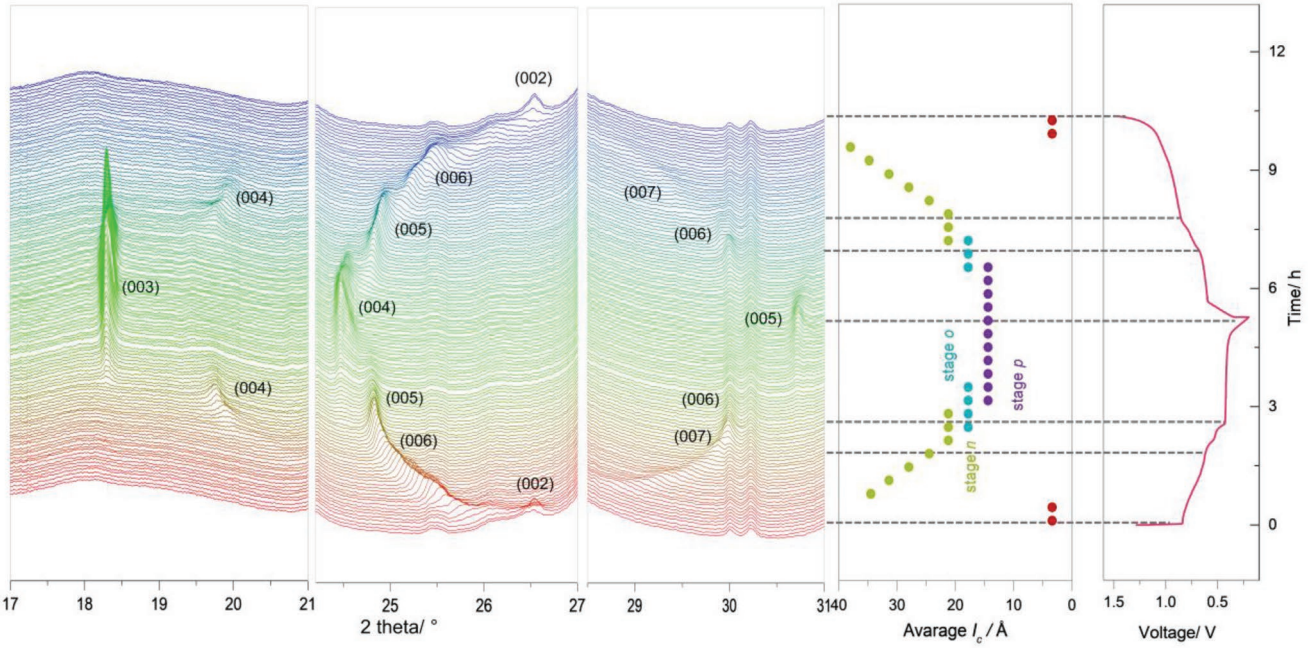

Figure 2. In situ synchrotron XRD analysis of the structural evolution of graphite during calciation and decalciation. Left: XRD patterns of graphite during discharging/charging; middle: lattice parameters (I_c) of intercalated/de-intercalated graphite; and right: the corresponding galvanostatic discharge/charge curve of a pouch cell. Note that items of *n*, *o*, and *p* stand for the integer number of graphene layers between two successive intercalated layers.

where d_{00l} and d_{00l+1} refer to the *d*-spacing values of the (00*l*) and (00*l* + 1) planes, respectively, and I_c is the *c* lattice parameter for the staging GIC, corresponding to the repeated distance. Accordingly, (00*l*), (00*l* +1), and I_c are shown in the left and middle panels of Figure 2, respectively. The I_c values for the stage *n*, *o*, and *p* GICs are 21.2, 17.8, and 14.4 Å, respectively, suggesting that the difference in I_c between adjacent GIC stages is ≈3.4 Å, similar to the interlayer distance of 3.35 Å for pristine graphite. This finding confirms that graphite undergoes a staging process during calciation, and that the *n*, *o*, and *p* GICs are consecutive phases. Considering the I_c of fully calciated graphite is less than five times the interlayer spacing of pristine graphite (14.4/3.35 = 4.30), *p* should not be greater than 4. Thus, {*n*, *o*, *p*} would be either {6, 5, 4}, {5, 4, 3}, {4, 3, 2}, or {3, 2, 1}. Note that the final stage *p* index can possibly be determined by studying the volume expansion of individual graphite sheets during electrochemical calciation. However, we failed to measure the precise volume change in our experiment because of the mechanical malleability of the fully calciated graphite sample. Later, we show that {*n*, *o*, *p*} is likely to be {4, 3, 2} with the aid of first-principles calculations.

In the following mechanistic study, we demonstrate that the calcium-ion intercalation into the graphite galleries was facilitated by the solvating molecules forming a ternary graphite compound. To verify the fully calciated structure, the graphite electrode was retrieved after the electrochemical discharge and examined using FTIR and ^{13}C-NMR spectroscopy. Figure S12 (Supporting Information) presents the FTIR spectrum of the electrode, which displays strong vibration peaks related to DMAc solvent molecules solvating calcium ions. This spectrum contrasts with that of the graphite sample that was simply soaked in the DMAc-based electrolyte or DMAc solvent, which did not display any signatures of DMAc molecules. This finding suggests that a significant amount of DMAc molecules solvating calcium ions is present in the discharged graphite electrode, and signifies the co-intercalation of calcium ions and DMAc into graphite galleries. To further examine the solvated Ca-ion structure and the nature of the calciated graphite, we conducted a ^{13}C-NMR study (**Figure 3**). The general ^{13}C-NMR spectra of the DMAc solvent, electrolyte, and calciated graphite contain four dominant peaks at similar positions, as shown in Figure 3a. For the DMAc solvent, the peaks are located at 20.5, 33.6, 36.7, and 168.9 ppm, corresponding to the four carbon atoms in a DMAc molecule, which are designated as 1, 2, 3, and 4, respectively (inset of Figure 3a).[21] For the DMAc-based electrolyte, we observed that the peak positions for 2, 3, and 4 shifted slightly to higher frequency (deshielding) at 33.8, 37.0, and 169.4 ppm, respectively, whereas a negligible change was observed for peak 1 (Figure 3b–d). The deshielding of carbon 2, 3, and 4 is attributed to the strong interaction between the electronegative O and N in DMAc and the electropositive calcium ion, leading to the inductive effect in neighboring C atoms, as schematically illustrated in the inset of Figure 3a. The presence of the DMAc that solvated the calcium ion could also be detected in the calciated graphite electrode with the characteristic ^{13}C-NMR shifts. Nevertheless, the peaks for each carbon 1, 2, 3, and 4 were further shifted and broadened, which is attributed to interactions with the host graphite and/or the randomness of orientations of DMAc molecules in the graphite slabs.[22] A few important points can be inferred from comparison of the ^{13}C-NMR spectra of the DMAc-based electrolyte and discharged graphite: namely, i) DMAc was co-intercalated with calcium ions into graphite galleries, and ii) the configuration of the solvated Ca ion intercalated into graphite differs from

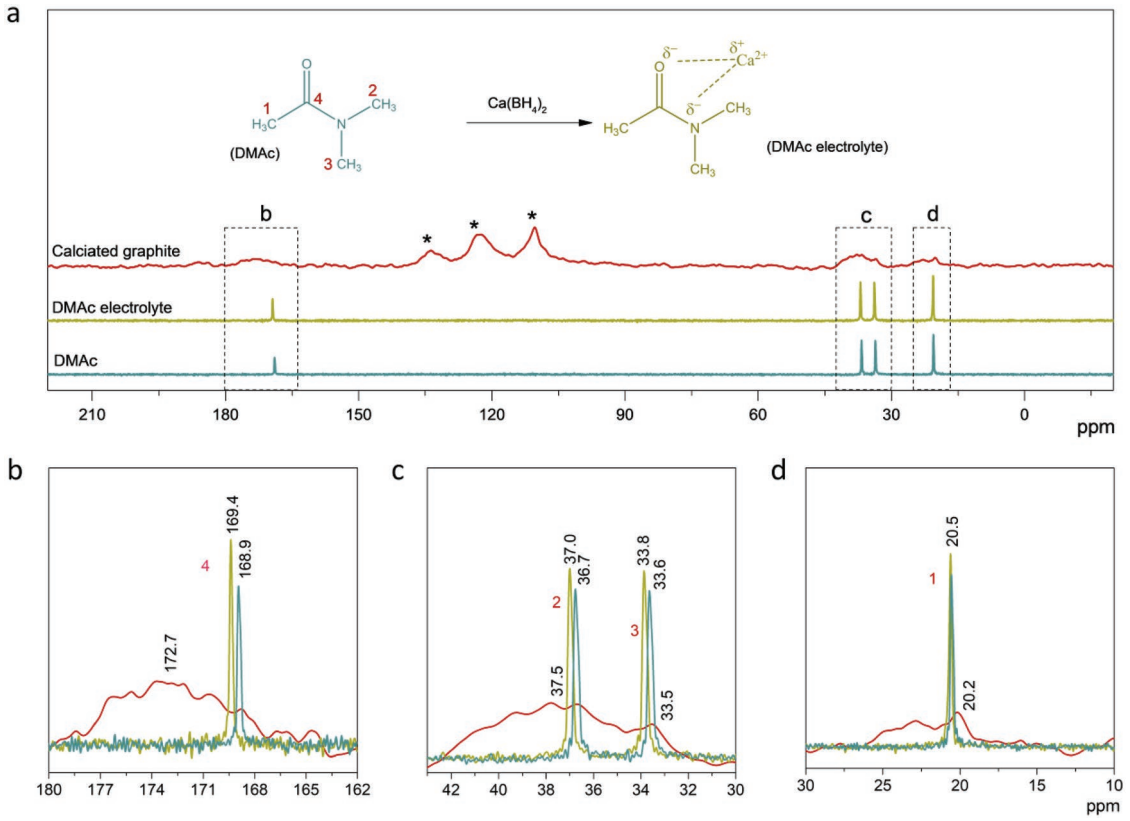

Figure 3. ^{13}C-NMR characterization of DMAc solvent, DMAc-based electrolyte, and fully discharged graphite. a) General NMR spectra, and chemical structure of DMAc molecule and the possible interaction between calcium ion and DMAc molecule in electrolyte, the four carbon atoms in DMAc molecule are designed as 1, 2, 3, and 4. b–d) Comparison of the positions of above designed four carbon signals in DMAc solvent, DMAc-based electrolyte, and fully discharged graphite. Note that three peaks at 109.8, 123, and 133.7 ppm indicated with * in (a) are from graphite or/and binder, which are attributable to the presence of aromatic rings from the edge of carbon.[21]

that in the electrolyte, as evidenced by the significant peak shift. Moreover, it should be noted that calcium intercalation using a solvent other than DMAc was not possible in the room-temperature calcium cell (Figure S1, Supporting Information), indicating that the unique solvation nature of DMAc could facilitate the calcium intercalation into graphite.

To further understand the solvated Ca-ion intercalation mechanism, we attempted to quantify the number of intercalated DMAc molecules per calcium ion in the graphite by monitoring the weight change of the graphite at various states of discharge and charge (**Figure 4**a). The graphite electrodes were carefully disassembled from the cells at each state of charge, followed by flushing with DMAc solvent and drying at 60 °C for 4 h in an Ar-filled glovebox. The dashed lines in Figure 4a indicate the theoretical weight change of graphite with potentially different numbers of DMAc molecules solvating calcium ions (b in Ca-(DMAc)$_b$). The experimentally measured weight changes followed the line assumed for $b = 4$, suggesting that one calcium ion is likely to be coordinated with four DMAc molecules during the intercalation. Note that the experimental values are slightly higher than the theoretical one, which can be attributed to the presence of irreversibly entrapped calcium ions.

Using first-principles calculations, we obtained a model structure of fully calciated graphite, considering the experimental capacity, solvation number of calcium ions, and XRD pattern analysis. It reveals that the graphite at the final calciated state is not likely to be in a stage 3 or stage 4 ordering, because they could not provide enough in-plane space for the accommodation of [Ca-(DMAc)$_4$] complexes to account for the observed discharge capacity. Structure optimization was thus performed more rigorously by considering only the stage 1 and stage 2 structures as the final calciated states, as shown in Figure S13 (Supporting Information) and Figure 4b. According to our calculations, the stage 1 and stage 2 GIC models consisted of repeating distances of ≈10 and ≈15.2 Å along the c-direction, respectively. Considering the experimental I_c value of 14.4 Å of the fully discharged electrode, this finding implies that the calciated graphite would be in the stage 2 GIC state, as shown in Figure 4b. To further confirm the plausibility of the proposed structure, we generated XRD patterns based on the model and compared them with the experimental observation. Figure 4c illustrates that not only the peak positions but also the peak intensities of the simulated spectrum corresponded well with the experimental ones, indicating that the structure in Figure 4b is an acceptable model. From this proposed model and XRD data, we figured out that the volume of the lattice during the intercalation reaction expands 215%, assuming the formation of a stage 2 GIC state with a 14.4 Å. Notably, this expansion is much smaller than the 347% volume change of Na–ether co-intercalated graphite.[23]

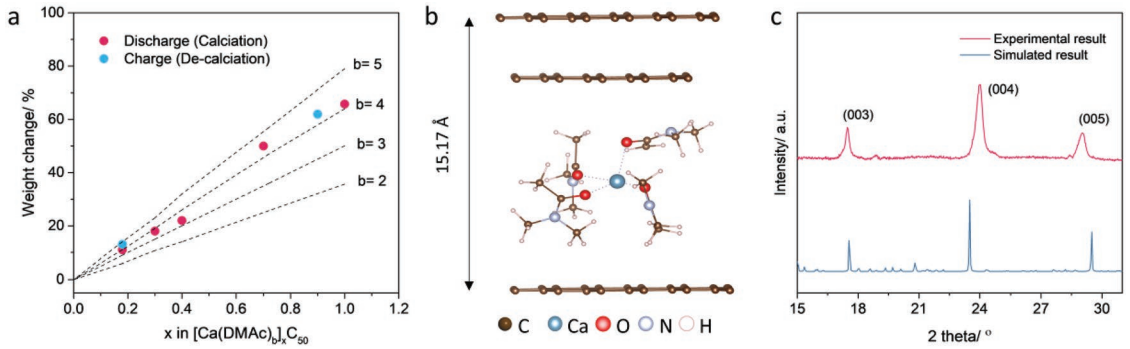

Figure 4. Analysis of the configuration of Ca-intercalated graphite. a) Weight change of graphite at various states of discharge and charge to determine to the molar ratio of DMAc:Ca intercalated in graphite galleries. b) DFT-simulated configuration of $[Ca(DMAc)_4]^{2+}$ co-intercalated graphite. c) XRD pattern of solvated-Ca-ion intercalated graphite compounds and the simulated XRD pattern of expanded graphite with repeated distance of 15.2 Å with the intercalant of $[Ca(DMAc)_4]^{2+}$ complex.

In this work, we reported, for the first time, that reversible calcium-ion insertion into graphite can occur electrochemically and reversibly at room temperature with the aid of a co-intercalating DMAc solvent. The graphite electrode in the CIBs delivered a reversible capacity of 85 mAh g^{-1} over 200 cycles with negligible degradation of the graphite. In situ XRD and electrochemical analyses revealed that the calciation occurs accompanying the staging process, which has generally been observed for lithium intercalation into graphite electrode. Moreover, structure analysis coupled with solid-state NMR and DFT calculations revealed that the fully calciated graphite formed stage 2 ternary GICs composed of a [Ca-$(DMAc)_4$] complex and layered graphite. This study offers useful insight into the development of CIBs, which has been retarded by the insufficient performance and sluggish kinetics of conventional electrode materials. Nudging calcium-ion intercalation into graphite host materials using co-intercalation chemistry will provide an unexplored pathway toward the realization of high-power and long-lasting CIBs.

Experimental Section

Preparation of Electrolytes: Electrolytes were prepared in an Ar-filled glovebox (O_2 < 0.5 ppm, H_2O < 0.5 ppm). Calcium salt ($Ca(BH_4)_2$, supplied by Aldrich) and molecular sieves were dried in a heating vacuum oven at 180 °C overnight. The dried $Ca(BH_4)_2$ was dissolved in DMAc, DEGDME, EC/DMC, and THF solvents at 0.5 M, respectively. The solutions were stirred at 50 °C for 8 h in the glove box before adding molecular sieves to further remove the H_2O in electrolytes.

Electrodes' Preparation and Electrochemical Characterizations: The graphite electrodes were prepared by mixing the natural graphite power (≈100 µm) and polyvinylidene fluoride (PVDF) binder at a mass ratio of 9:1 before adding desirable amount of *N*-methyl-2-pyrrolidone solvent. The uniform mixture was then cast on Cu foil and dried at 70 °C in a vacuum oven. The graphite electrodes were cut into disks with a diameter of 3/8 in. and an active mass loading of about 3 mg cm^{-2}. Ca metal powders were pressed into pellets and polished before using as the counter electrodes. CR2032 coin cells were assembled in an Ar-filled glovebox using graphite as working electrodes, Ca metal pellets as counter electrodes, and glass fiber as separators filled with as-prepared electrolytes. The coin cells were tested on a multichannel potentio-galvanostat (Won A Tech, Korea) at different current densities ranging from 0.2 to 1.5 V. The *CV* curves were measured at scan rates ranging from 0.025 to 1 mV s^{-1} between 0.2 and 1.5 V.

Material Characterizations: For in situ XRD study, pouch cells were prepared with graphite working electrodes, Ca metal pellets as counter electrodes, and Celgard separators filled with DMAc-based electrolyte. In situ XRD experiment was operated on a 3D XRD beamline at PLS-II with a wavelength of λ = 0.8265 Å (Pohang Accelerator Laboratory, Korea), and the XRD data were collected as a set of circles on a Mar 345-image plate detector in transmission mode for ≈1 min exposure time. Taking the scanning time of the image and the transferring time of the data into account, the period between two data recording was about 5 min. Note that for convenient comparison with the literature, all the two θ angles from the raw XRD data were recalculated to corresponding angles for λ = 1.543 Å, the wavelength of the general X-ray tube sources with Cu Kα radiation. The morphology of cycled electrodes was evaluated by scanning electron microscopy (SEM, Supra 55VP, Carl Zeiss, Germany). Ca storage mechanisms were also studied by XPS (PHI 5000 VersaProbe, ULVAC PHI, Japan), Raman (Horiba Jobin Yvon LabRam Aramis, Horiba, France), and FTIR (FT-IR-4200, JASCO, Japan). HR-TEM (JEM-F200, Jeol, Japan) and 500 MHz WB solid NMR (Advance III HD, Bruker, German) analyses were conducted at the National Center for Inter-university Research Facilities (NCIRF) at Seoul National University. To determine the *b* value in Ca-$(DMAc)_b$ ion complex, cycled electrodes were dissembled, washed with DMAc, and dried at 60 °C in an Ar-filled glove box before measuring their weights. Six samples were prepared for each point and the average values were plotted accordingly.

Simulation Methods: Density functional theory calculations were conducted to obtain information on the structure of Ca-DMAc co-intercalated graphite. Projector-augmented wave pseudopotentials[24] were used as implemented in Vienna Ab initio Simulation Package,[25] and Perdew–Burke–Ernzerhof exchange-correlation functional[26] was applied for all calculations. Van der Waals interactions were considered with the DFT-D3 method,[27] and the geometry optimization with a kinetic energy cutoff of 500 eV was performed until the remaining force of the system converged within 0.01 eV $Å^{-1}$.

Supporting Information

Supporting Information is available from the Wiley Online Library or from the author.

Acknowledgements

This work was supported by the National Research Foundation of Korea (NRF) grant funded by the Korea government (MSIP) (No. 2018R1A2A1A05079249); the Supercomputing Center/Korea Institute of Science and Technology Information with supercomputing resources

including technical support (KSC-2016-C3-0069); and Project Code (IBS-R006-A2). This research was partly supported by Shell company. Z.-L.X acknowledges the Korea Research Fellowship (KRF) Program through the National Research Foundation of Korea (NRF) (Project No. 2017H1D3A1A01013931).

Note: The name of the author Jian Wang was presented incorrectly in the author line when the article was first published online as Jiang Wang. This was corrected on January 27, 2020.

Conflict of Interest

The authors declare no conflict of interest.

Author Contributions

J.P., Z.-L.X., and G.Y. contributed equally to this work. K.K., J.P., and Z.-L.X. conceived the idea; Z.-L.X. and J.P. conducted the electrochemical experiments, material characterizations, and in situ XRD work; and G.Y. carried out the DFT calculations. Y.-J.K. conducted NMR analysis. S.K.P., J.W., H.H., H.P., J.L., and Y.S.Y. contributed to the characterizations and preparation of the manuscript. K.K. guided the project and revised the manuscript prepared by the first authors. All the authors commented on the manuscript.

Keywords

anode materials, calcium-ion batteries, graphite

Received: July 10, 2019
Revised: October 17, 2019
Published online: November 18, 2019

[1] a) M. Armand, J. M. Tarascon, *Nature* **2008**, *451*, 652; b) M. S. Whittingham, *Chem. Rev.* **2014**, *114*, 11414; c) K. Kang, Y. S. Meng, J. Bréger, C. P. Grey, G. Ceder, *Science* **2006**, *311*, 977.

[2] D. Aurbach, Z. Lu, A. Schechter, Y. Gofer, H. Gizbar, R. Turgeman, Y. Cohen, M. Moshkovich, E. Levi, *Nature* **2000**, *407*, 724.

[3] J. Muldoon, C. B. Bucur, T. Gregory, *Chem. Rev.* **2014**, *114*, 11683.

[4] a) M.-C. Lin, M. Gong, B. Lu, Y. Wu, D.-Y. Wang, M. Guan, M. Angell, C. Chen, J. Yang, B.-J. Hwang, H. Dai, *Nature* **2015**, *520*, 324; b) D. J. Kim, D.-J. Yoo, M. T. Otley, A. Prokofjevs, C. Pezzato, M. Owczarek, S. J. Lee, J. W. Choi, J. F. Stoddart, *Nat. Energy* **2019**, *4*, 51.

[5] a) R. Y. Wang, B. Shyam, K. H. Stone, J. N. Weker, M. Pasta, H.-W. Lee, M. F. Toney, Y. Cui, *Adv. Energy Mater.* **2015**, *5*, 1401869; b) J. W. Choi, D. Aurbach, *Nat. Rev. Mater.* **2016**, *1*, 16013.

[6] A. Ponrouch, C. Frontera, F. Bardé, M. R. Palacín, *Nat. Mater.* **2016**, *15*, 169.

[7] M. Wang, C. Jiang, S. Zhang, X. Song, Y. Tang, H.-M. Cheng, *Nat. Chem.* **2018**, *10*, 667.

[8] D. Wang, X. Gao, Y. Chen, L. Jin, C. Kuss, P. G. Bruce, *Nat. Mater.* **2018**, *17*, 16.

[9] D. Kim, J. H. Ryu, *Electron. Mater. Lett.* **2019**, *15*, 415.

[10] R. J. Gummow, G. Vamvounis, M. B. Kannan, Y. He, *Adv. Mater.* **2018**, *30*, 1801702.

[11] D. S. Tchitchekova, D. Monti, P. Johansson, F. Bardé, A. Randon-Vitanova, M. R. Palacín, A. Ponrouch, *J. Electrochem. Soc.* **2017**, *164*, A1384.

[12] a) Z. Rong, R. Malik, P. Canepa, G. Sai Gautam, M. Liu, A. Jain, K. Persson, G. Ceder, *Chem. Mater.* **2015**, *27*, 6016; b) X. Sun, P. Bonnick, V. Duffort, M. Liu, Z. Rong, K. A. Persson, G. Ceder, L. F. Nazar, *Energy Environ. Sci.* **2016**, *9*, 2273; c) X. Sun, P. Bonnick, L. F. Nazar, *ACS Energy Lett.* **2016**, *1*, 297.

[13] R. Fong, U. von Sacken, J. R. Dahn, *J. Electrochem. Soc.* **1990**, *137*, 2009.

[14] a) L. B. Ebert, *Annu. Rev. Mater. Sci.* **1976**, *6*, 181; b) Z.-L. Xu, J. Park, G. Yoon, H. Kim, K. Kang, *Small Methods* **2019**, *3*, 1800227; c) Z.-L. Xu, G. Yoon, K.-Y. Park, H. Park, O. Tamwattana, S. J. Kim, W. M. Seong, K. Kang, *Nat. Commun.* **2019**, *10*, 2598.

[15] a) X.-T. Xi, X. Feng, X.-J. Nie, B.-H. Hou, W.-H. Li, X. Yang, A.-B. Yang, W.-D. Sun, X.-L. Wu, *Chem. Commun.* **2019**, *55*, 8406; b) W.-H. Li, Q.-L. Ning, X.-T. Xi, B.-H. Hou, J.-Z. Guo, Y. Yang, B. Chen, X.-L. Wu, *Adv. Mater.* **2019**, *31*, 1804766.

[16] N. Emery, C. Hérold, M. d'Astuto, V. Garcia, C. Bellin, J. F. Marêché, P. Lagrange, G. Loupias, *Phys. Rev. Lett.* **2005**, *95*, 087003.

[17] W. Xu, M. M. Lerner, *Chem. Mater.* **2018**, *30*, 6930.

[18] J. A. Seel, J. R. Dahn, *J. Electrochem. Soc.* **2000**, *147*, 892.

[19] H. Kim, K. Lim, G. Yoon, J.-H. Park, K. Ku, H.-D. Lim, Y.-E. Sung, K. Kang, *Adv. Energy Mater.* **2017**, *7*, 1700418.

[20] Z.-L. Xu, K. Lim, K.-Y. Park, G. Yoon, W. M. Seong, K. Kang, *Adv. Funct. Mater.* **2018**, *28*, 1802099.

[21] a) W. Cai, R. D. Piner, F. J. Stadermann, S. Park, M. A. Shaibat, Y. Ishii, D. Yang, A. Velamakanni, S. J. An, M. Stoller, J. An, D. Chen, R. S. Ruoff, *Science* **2008**, *321*, 1815; b) M. Mermoux, Y. Chabre, A. Rousseau, *Carbon* **1991**, *29*, 469; c) W. F. Reynolds, S. McLean, L.-L. Tay, M. Yu, R. G. Enriquez, D. M. Estwick, K. O. Pascoe, *Magn. Reson. Chem.* **1997**, *35*, 455; d) J. C. C. Freitas, F. G. Emmerich, G. R. C. Cernicchiaro, L. C. Sampaio, T. J. Bonagamba, *Solid State Nucl. Magn. Reson.* **2001**, *20*, 61.

[22] N. Leifer, M. F. Greenstein, A. Mor, D. Aurbach, G. Goobes, *J. Phys. Chem. C* **2018**, *122*, 21172.

[23] H. Kim, J. Hong, G. Yoon, H. Kim, K.-Y. Park, M.-S. Park, W.-S. Yoon, K. Kang, *Energy Environ. Sci.* **2015**, *8*, 2963.

[24] a) P. E. Blöchl, *Phys. Rev. B* **1994**, *50*, 17953; b) G. Kresse, D. Joubert, *Phys. Rev. B* **1999**, *59*, 1758.

[25] G. Kresse, J. Furthmüller, *Comput. Mater. Sci.* **1996**, *6*, 15.

[26] J. P. Perdew, K. Burke, M. Ernzerhof, *Phys. Rev. Lett.* **1996**, *77*, 3865.

[27] S. Grimme, J. Antony, S. Ehrlich, H. Krieg, *J. Chem. Phys.* **2010**, *132*, 154104.